Distribution of Tropical Tropospheric Water Vapor

DE-ZHENG SUN AND RICHARD S. LINDZEN

Center for Meteorology and Physical Oceanography, Massachusetts Institute of Technology, Cambridge, Massachusetts

(Manuscript received 30 December 1991, in final form 11 August 1992)

ABSTRACT

Utilizing a conceptual model for tropical convection and observational data for water vapor, the maintenance of the vertical distribution of the tropical tropospheric water vapor is discussed. While deep convection induces large-scale subsidence that constrains the turbulent downgradient mixing to within the convective boundary layer and effectively dries the troposphere through downward advection, it also pumps hydrometeors into the upper troposphere, whose subsequent evaporation appears to be the major source of moisture for the large-scale subsiding motion. The development of upper-level clouds and precipitation from these clouds may also act to dry the outflow, thus explaining the low relative humidity near the tropopause. A one-dimensional model is developed to simulate the mean vertical structure of water vapor in the tropical troposphere. It is also shown that the horizontal variation of water vapor in the tropical troposphere above the trade-wind boundary layer can be explained by the variation of a moisture source that is proportional to the amount of upper-level clouds. Implications for the nature of water vapor feedback in global warming are discussed.

1. Introduction

Chief among the greenhouse gases in the atmosphere is water vapor. The impact of water vapor on climate arises primarily from the water vapor above the boundary layer. Unfortunately, there is a lack of adequate data for water vapor in the upper troposphere. There is also considerable uncertainty about the processes that maintain the water vapor distribution (Lindzen 1990a,b; Betts 1990). With respect to the former, recent satellite measurements of upper-tropospheric water vapor have improved the situation (Rind et al. 1991).

The large-scale distribution of water vapor is dependent on the properties of moist convection. Though we still do not have an adequate understanding of the anatomy of moist convection and how it interacts with the large-scale flow, we do have much relevant information, especially through the GATE experiment (Houze and Betts 1981). This paper attempts to describe in a coherent manner the observed distribution of water vapor as well as our conceptual understanding of moist convection and its interplay with the large-scale circulation. We wish to identify the most important physical processes and their roles in maintaining the large-scale water vapor distribution.

Our attention here is focused on the tropical troposphere. We begin with observations of the vertical and meridional distributions of water vapor. Using a conceptual model, we describe the roles of deep cloud-induced subsidence and of evaporation of hydrometeors[1] in maintaining the vertical distribution of water vapor. We then discuss the meridional variation and the role of the Hadley circulation. In section 3, we present a one-dimensional (horizontally averaged) model that simulates the observed vertical structure of tropical tropospheric water vapor. In section 4, we present a two-dimensional model that explains the meridional variation of the relative humidity throughout the free troposphere (the troposphere above the convective boundary layer). Section 5 provides a summary.

2. The observed vertical and meridional distribution of water vapor

a. The vertical distribution and the role of evaporation of hydrometeors

To form a framework for understanding the observed water vapor distribution, we start from a heuristic model for the vertical structure of tropical convection. It is schematically illustrated in Fig. 1. In this picture, tropical convection is idealized into two kinds of clouds: deep precipitating clouds and shallow nonprecipitating clouds. Nonprecipitating clouds moisten the convective boundary layer, which supplies the fuel for the deep convection.

Corresponding author address: Dr. Richard S. Lindzen, Center for Meteorology and Physical Oceanography, Massachusetts Institute of Technology, Cambridge, MA 02139.

[1] Hydrometeors throughout this article refer to the liquid or ice particles that exist outside of saturated cumulus updrafts.

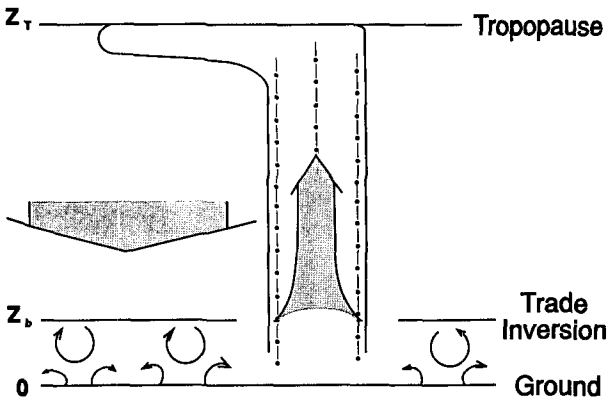

FIG. 1. A schematic illustration of the historical picture of tropical convection and its associated circulation.

The deep convection induces large-scale subsidence, which suppresses the shallow convection. The interaction of the two kinds of convection thus provides a coherent picture. This picture was first envisioned by Riehl and collaborators in studying the energy budget of the tropical convergence zone and the trade-wind regime (Riehl et al. 1957; Riehl and Malkus 1958, 1979). Schneider (1977) used it to estimate the mean stability of the mean thermal structure of the whole Hadley domain, and Sarachik (1978) used it as a basis to form a one-dimensional coupled ocean–atmosphere model. Most recently, in the context of radiative convective equilibrium, Betts and Ridgway (1991) and Sun and Lindzen (1992) showed that this simple picture is able to depict the main characteristics of the vertical structure of tropical tropospheric temperature.

The aforementioned works were concerned with the energy budget rather than the determination of humidity. Little attention had to be paid to the evaporation of hydrometeors and precipitation efficiency of individual clouds. This is also reflected in a mechanism of water vapor feedback proposed by Lindzen (1990a,b). In those papers, it was assumed that all condensed water vapor in deep clouds falls to the ground as rain and the water vapor source for the free tropospheric air is the detrainment of saturated air from the deep cloud top. This assumption has been questioned by Betts (1990). In the present paper, we will see more clearly that the evaporation of hydrometeors has to be taken into account in order to properly deal with the vertical distribution of water vapor. The simple descent of a saturated parcel leads rapidly to lower relative humidities than are observed.

The above picture can be interpreted as the averaged vertical structure for the whole Hadley domain (Lindzen 1990b). Figures 2 and 3 present the observed vertical distribution of relative humidity averaged for the Hadley circulation domain for both January and July. In Fig. 2, the relative humidity is with respect to water saturation, while in Fig. 3 the relative humidity above the height of the melting level is with respect to ice saturation. Conventional sounding data (Oort 1983) and recent satellite data for the clear sky (SAGE II data for the year 1987; see Rind et al. 1991) are both presented. Conventional sounding of water vapor ends around 300 mb and satellite measurements cannot probe the low troposphere frequently enough to form a representative sample. In the region where both overlap, the satellite data reveal a much drier troposphere than the sounding data. Though it is expected that clear-sky conditions should be drier than average (including both cloudy sky and clear sky), the difference is still striking. As discussed in Rind et al. (1990), the water vapor distribution obtained by SAGE II has been validated by comparison with radiosonde data, frost point hygrometer, Lyman-α, and LIMS satellite observations, and has been shown to have an estimated accuracy of about 10%. Though there are still uncertainties in SAGE II data, it is also possible that the conventional sounding data may exaggerate the actual water vapor content of the air. Conventional sondes generally do not report when the relative humidity is

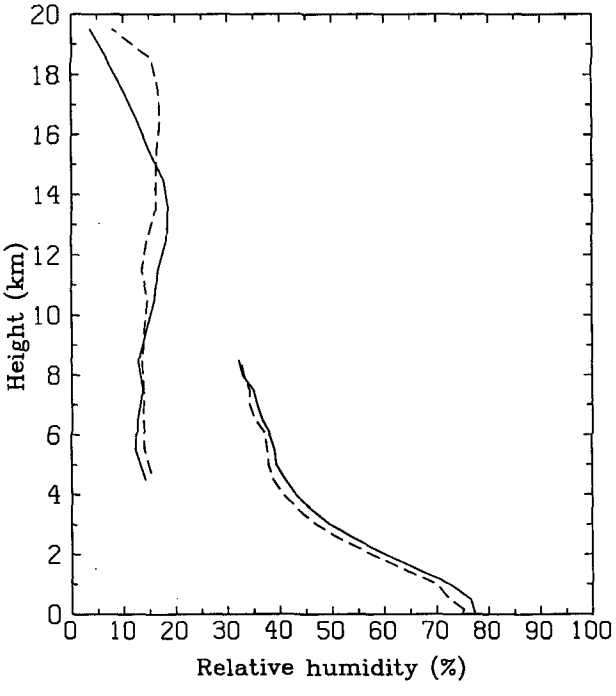

FIG. 2. The vertical structure of the observed water vapor distribution averaged over the domain of the Hadley circulation. Relative humidity is with respect to liquid water. The satellite data and conventional data are both presented. The solid line is for the month of January, and the dashed line is for the month of July. (The region over which data was averaged was 15°S to 25°N for January and 25°S to 15°N for July.) Averaged relative humidity was obtained through the averaged water vapor mixing ratio and the averaged temperature. The satellite data for water vapor mixing ratio is from the SAGE II measurements. The conventional data for water vapor mixing ratio and temperature (used to obtain relative humidity) are from Oort (1983).

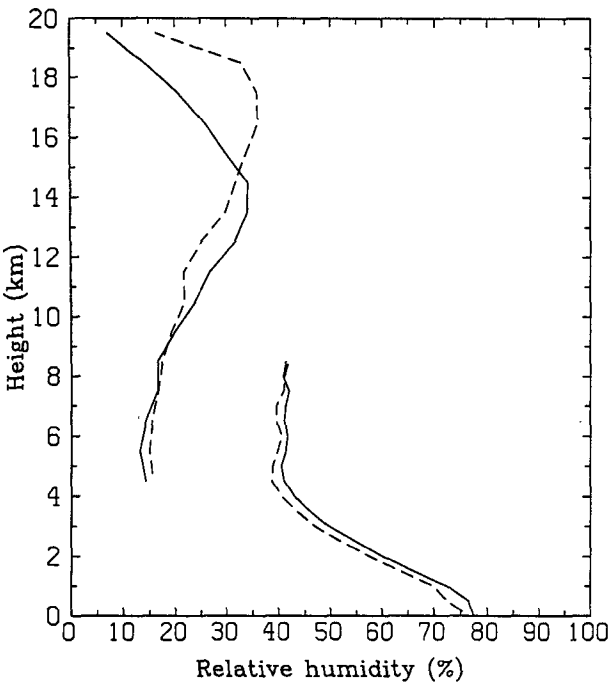

FIG. 3. Same as Fig. 2 but above the melting level the relative humidity is with respect to ice saturation.

below 20% (Starr and Melfi 1990). Also, since the water vapor content decreases with height exponentially with a scale height of about 2–3 km, the sonde may report an exaggerated relative humidity due to contamination. It is worth noting that some detailed soundings in the trade-wind regime do show the relative humidity immediately above the trade inversion falling to 20% (Riehl 1979). We here assume that the two datasets give bounds on the actual water vapor content for average conditions.

There are two features in the vertical distribution of tropical tropospheric water vapor to be noted. First, throughout the troposphere, the air is subsaturated. Second, the relative humidity with respect to ice in the upper troposphere is low and does not drop much on the way to the low atmosphere (the relative humidity with respect to water saturation remains fairly constant or increases with the decrease of height). In the absence of any macroscale circulation, the atmosphere would eventually saturate due to molecular diffusion. The first feature indicates the importance of macroscale circulations. The second feature illustrates the necessity of including the evaporation of hydrometeors in the picture shown in Fig. 1.

The mean detrainment level for the cumulonimbus towers is about 200 mb where the water vapor that a unit mass of air can hold will be less than 0.1 g kg^{-1} (the saturation water mixing ratio with respect to ice). Therefore, if in the process of the air going poleward and subsiding, it does not get more water vapor from any other source, the observed vertical structure over the tropics will be characterized by a constant mixing ratio of 0.1 g kg^{-1} from 200 mb to the height of the trade inversion. This also means an exponential decrease of relative humidity away from the tropopause to the low atmosphere with a scale height of about 3 km. The observed profile is far different from this and indicates the presence of a water vapor source in the subsiding air.

It should be noted that just as the source of water vapor for the free troposphere cannot be the subsidence of detrained saturated air, so too, the required water vapor source cannot be the diffusive transport of water vapor from below. The diffusive transport is largely restricted to below the trade inversion. This is evident in the thermal and moisture structure across the top of the trade inversion where both the water vapor and temperature have a discontinuity (Augstein et al. 1974; Riehl 1979). Note that due to the adiabatic cooling, a lifted air parcel will be saturated within a kilometer or so of its origin. Thus, neither can the water vapor source be supplied by the large-scale lifting of moist air from the low atmosphere since we do not see large-scale deep cloud cover over the whole tropics.

The water vapor source has to ultimately come from deep convection. Considering the fact that deep convection in the tropics generates widespread upper-level clouds and these upper-level clouds generate precipitation that falls through a subsaturated environment (Houze and Betts 1981), the leading candidate for moistening the subsiding air seems to be the evaporation of precipitation generated by upper-level clouds. The low value of relative humidity near the tropopause further implies that some mechanism is needed to dry out the outflow of deep convective towers. This mechanism is likely provided by the formation of upper-level clouds. The upper-level clouds generate precipitation that falls from the outflow and generates regions with subsiding motion. Subsaturation can occur in the region of the subsiding motion.

The formation and the life cycle of the upper-level clouds have not been well understood, but it is worth noting the role of radiation. As discussed by Danielsen (1982), the difference of the radiative cooling rate between the cloud top and bottom helps to maintain the convective overturning within the clouds and generate more precipitating particles. This mechanism was originally proposed to explain the dryness of the low stratospheric air.

In the next subsection, we will present a budget study that further suggests that evaporation of precipitation from upper-level clouds is the major moisture source of the large-scale subsiding motion.

b. A budget study for the free tropospheric water vapor

The tropical rainfall is mostly provided by the mesoscale rain systems described by Houze (1989). The

budget study of the mesoscale rain system shows that the amount of water substance carried out of the mesoscale cloud cluster (the edge of the anvil) by the outflow is about 12% of the total rainfall produced by the whole mesoscale system (Gamache and Houze 1983). For the month of January, the rain averaged over the whole Hadley cell (say, from 15°S to 25°N) is estimated to be about 4.8×10^{-5} kg m^{-2} s^{-1} (Riehl 1979). Therefore, averaged over the month of January and over the Hadley cell, the deposit of moisture in the troposphere through the outflow of the mesoscale system occurs at a rate of about 5.8×10^{-6} kg m^{-2} s^{-1}.

The sink of water vapor of the large-scale flow is the downward advection by deep cloud-induced subsidence, which can be estimated by the energy budget of the subsidence wherein the subsidence heating is primarily balanced by radiative cooling. At 4.5 km, for example, the corresponding subsidence is estimated to be about 2.0×10^{-3} kg m^{-2} s^{-1} [radiative cooling rate is taken from Dopplick (1972)]. The removal of water vapor by the subsidence from the troposphere above 4.5 km is about 5.2×10^{-6} kg m^{-2} s^{-1} or 2.2×10^{-6} kg m^{-2} s^{-1} depending on if the satellite data or the conventional sounding data is used. These numbers suggest that the moisture carried out of the anvil is sufficient to keep the air as moist as observed to below 4.5 km.

The other source of water vapor is the mixing associated with the dissipation of deep convective towers. This source for water vapor may be estimated as follows. Suppose the deep convective tower is active for a characteristic time τ and then begins to dissipate; the moisture source per unit area it provides is

$$\frac{\sigma}{\tau}\int \rho(q^* + l^* - q_m)dz,$$

where q^* is the water vapor mixing ratio of cloud air, l^* is the cloud water content in the dissipating stage, q_m is water vapor mixing ratio of the surrounding air where the deep convective towers are generated, and σ is the fractional area covered by active clouds. Integration is for the region of interest. Here $\sigma \sim 10^{-3}$ (note velocity within the deep convective tower is about three orders of magnitude larger than the mean subsidence over the Hadley circulation), τ is about an hour, and l^* is about 0.2 g kg^{-1} (Braham 1952). Taking the region between the tropopause and 4.5 km and assuming q_m can be replaced by the mixing ratio of the mean flow over the scale of the Hadley circulation, the rate of moisture input through dissipation of deep clouds is estimated to be between 2.0×10^{-6} kg m^{-2} s^{-1} and 2.5×10^{-6} kg m^{-2} s^{-1} depending on whether the conventional data or the satellite data are used. It should be noted that q_m can be much larger than the mixing ratio of the mean flow over the scale of the Hadley circulation. Furthermore, the dissipating stage of deep clouds is usually accompanied by cloud-scale downdrafts, which may act to effectively remove the water substance within the clouds. The above numbers may greatly overestimate the contribution to the large-scale humidity from the dissipation of deep convective towers. Nevertheless, this effect may not be completely negligible in view of Braham's budget study and Emanuel's scheme for cumulus parameterization (Braham 1952; Emanuel 1991).

Dissipation of clouds including deep convective towers and upper-level clouds is accompanied by evaporation of hydrometeors. Evaporation of hydrometeors occurs at the edge of clouds. Observations of tropical rain systems further show that dissipation of clouds is characterized by a gradual elevation of the cloud base. While their bases are rising, clouds continue to generate precipitation, which falls into the subsaturated air below the cloud base and evaporates (Johnson and Young 1983). The role of the evaporation of hydrometeors is the focus of this paper.

Before we further quantify the above processes, we turn to the meridional distribution of water vapor over the whole Hadley domain. Features in the horizontal variation offer further information about the distributions of sinks and sources of water vapor.

c. *The meridional distribution and the role of the Hadley circulation*

Figures 4–7 show the zonal mean specific humidity and relative humidity fields for July and January. Though the satellite data [SAGE II data for the year 1987 (Rind et al. 1991)] reveal a much drier middle

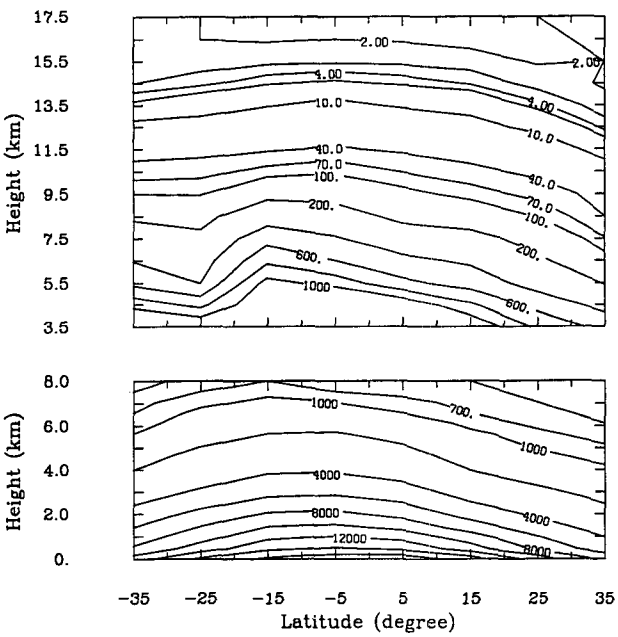

FIG. 4. Meridional distribution of tropical tropospheric water vapor mixing ratio in January (in units of 10^{-3} g kg^{-1}). Upper panel: satellite data. Lower panel: conventional data.

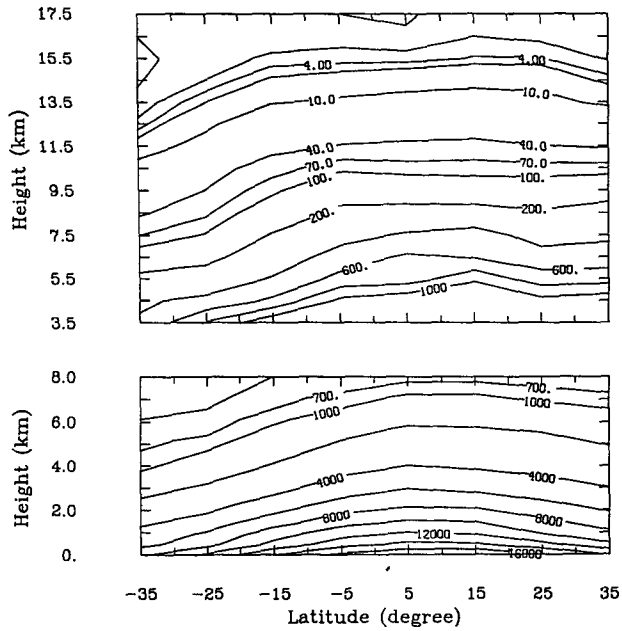

FIG. 5. Meridional distribution of tropical tropospheric water vapor mixing ratio in July (in units of 10^{-3} g kg^{-1}). Upper panel: satellite data. Lower panel: conventional data.

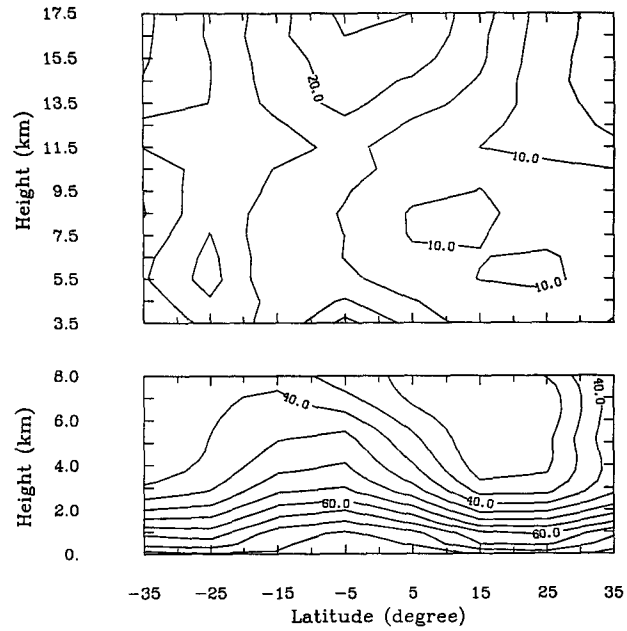

FIG. 6. Meridional distribution of tropical tropospheric relative humidity (with respect to liquid water) in January. Upper panel: satellite data. Lower panel: conventional data.

troposphere than the conventional data (Oort 1983), they both show the distribution of water vapor to be strongly modulated by the zonal mean meridional circulation. Figure 8 shows the zonal mean meridional circulation for July and January. The air in the downward portion of the Hadley circulation is much drier than the air in the upward portion.[2]

The water vapor budget equation for the monthly mean Hadley circulation may be written as

$$\rho\frac{\partial[\bar{q}]}{\partial t}+\rho[\bar{w}]\frac{\partial[\bar{q}]}{\partial z}+\rho[\bar{v}]\frac{\partial[\bar{q}]}{\partial y}$$

$$=[\bar{E}]+[\bar{M}_c]\frac{\partial[\bar{q}]}{\partial z}-\left[\overline{q'\frac{\partial M_c'}{\partial z}}\right]-\left[\bar{q}^*\frac{\partial\bar{M}_c^*}{\partial z}\right]-\frac{\partial\rho[\overline{v'q'}]}{\partial y}-\frac{\partial\rho[\bar{v}^*\bar{q}^*]}{\partial y}-\frac{\partial\rho[\overline{w_e'q'}]}{\partial z}-\frac{\partial\rho[\bar{w}_e^*\bar{q}^*]}{\partial z}; \quad (1)$$

"$\bar{}$" represents the time average, "$'$" and "$*$" represent the deviations from the time mean and zonal mean, respectively, q is the mean water vapor mixing ratio, w is the vertical velocity, M_c is the net convective mass flux associated with moist convection, w_e is the vertical velocity in the environment of moist convection ($\rho w_e = \rho w - M_c$), E is the moistening from convection due to evaporation of hydrometeors and dissipation of clouds, and ρ is the air density; z and y represent the height and the latitude, respectively. A formal derivation is presented in the Appendix. Problems and limitations in previous formulations of the water vapor and heat budget of a large-scale flow embedding moist convection are discussed in some detail there.

Within the domain of the Hadley circulation, the horizontal transport by eddies (both transient and steady) is negligible compared with the horizontal advection by the mean circulation (Newell et al. 1982). The last two terms represent the vertical eddy transport in the environment of moist convection, which we may also assume negligible compared with the vertical transport by moist convection (or the vertical advection by the mean circulation). Above the convective boundary layer and away from the immediate region of the tropopause, the vertical variation of M_c is much smaller than the vertical variation of q (Ogura and Cho 1973). Therefore, we may further neglect the eddy transport associated with the vertical variation of M_c.

[2] For purposes of climate feedbacks, the relevant quantity is the specific humidity averaged over the entire Hadley circulation, which, it should be noted, extends as a single cell across the whole tropics (Lindzen and Hou 1988). There is no evidence of any significant change in this quantity between January and July.

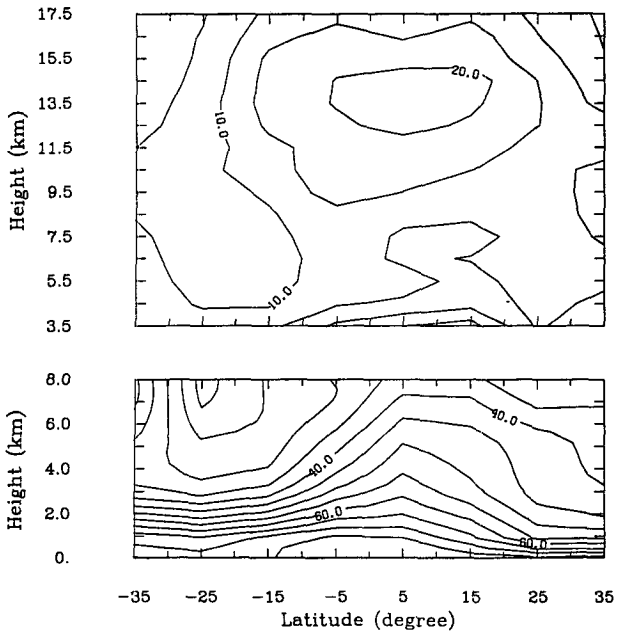

FIG. 7. Meridional distribution of tropical tropospheric relative humidity (with respect to liquid water) in July. Upper panel: satellite data. Lower panel: conventional data.

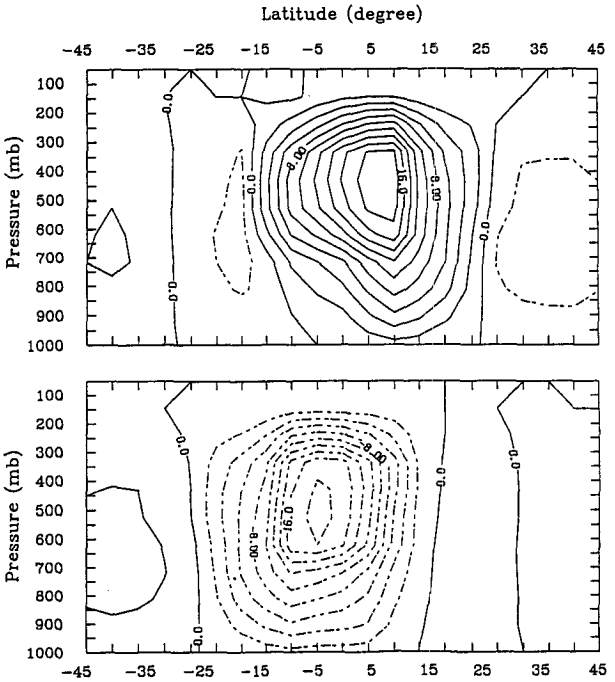

FIG. 8. Streamlines of the Hadley circulation (in units of 10^{10} kg s^{-1}). Data is from Oort (1983). Upper panel: January. Lower panel: July. The direction of the circulation is indicated by different line types. Solid line: clockwise. Dashed line: counterclockwise.

Ignoring the monthly mean tendency, equation (1) is simplified to

$$0 = -\left(\rho[\bar{w}]\frac{\partial[\bar{q}]}{\partial z} + \rho[\bar{v}]\frac{\partial[\bar{q}]}{\partial y}\right) + [\bar{M}_c]\frac{\partial[\bar{q}]}{\partial z} + [\bar{E}]. \quad (2)$$

The sum of the meridional and vertical advection by the Hadley circulation is shown in Fig. 9. Monthly mean data were used in the calculation. Due to the much larger vertical gradient of the water vapor mixing ratio, the meridional transport is an order of magnitude smaller than the vertical transport in most regions of the Hadley circulation. Therefore, zonal mean circulation alone generates an excess of water vapor within the rising branch and a deficit of water vapor within the subsiding branch. By Eq. (2), it is evident that the moist convection acts as a sink in the upward portion and a source term in the region of downward motion. In the intertropical convergence zone (ITCZ) (upward portion), where moist convection is concentrated, E is positive and significant. Therefore, M_c must be larger than w there (note $\rho[\bar{w}]\{\partial[\bar{q}]/\partial z\} \gg \rho[\bar{v}]\{\partial[\bar{q}]/\partial y\}$). What this means is that a percentage of the air pumped into the upper troposphere by deep convection subsides within the ITCZ. Gray (1974) reached the same conclusion in analyzing the water vapor budget of a cloud cluster region. Our picture of the ITCZ results from a spatial average over a scale much larger than the scale of deep convective clouds. In between these deep convective towers is subsiding motion. The concentration of deep convection itself is controlled by the sea surface temperature distribution (Lindzen and Nigam 1987). In the subtropics

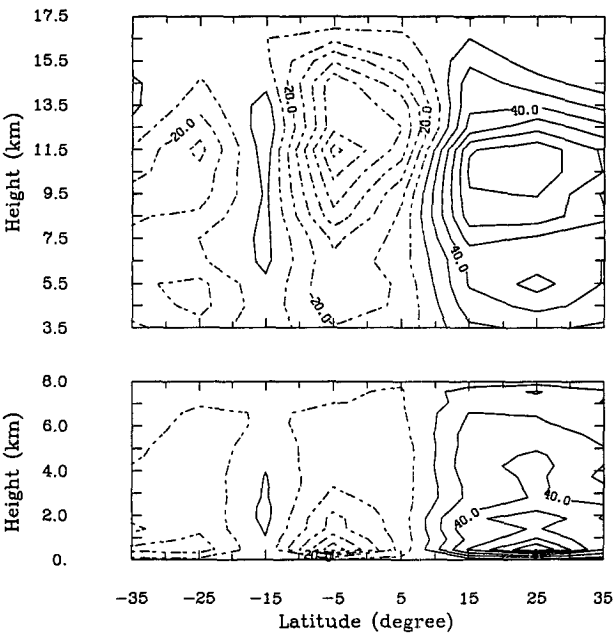

FIG. 9. $([\bar{w}]\{\partial[\bar{q}]/\partial z\} + [\bar{v}]\{\partial[\bar{q}]/\partial y\})/[\bar{q}]$ for January (yr^{-1}). Data for the meridional circulation is from Oort (1983). Upper panel: satellite data. Lower panel: conventional data.

(downward portion), large-scale subsidence prevails, and deep convection is largely suppressed, but there is still a considerable amount of deep convection in the subtropics as indicated by the upper-level cloud cover (Barton 1983).

In the following section, we will try to quantify the discussed processes and formulate a mathematical model in order to further assess the role of convection in maintaining the observed distribution, especially the interplay between the subsidence drying and the moistening from the evaporation of hydrometeors.

3. A model for the mean vertical structure of the tropical tropospheric water vapor

The model structure is schematically shown in Fig. 10. In the vertical, the troposphere is divided into three different regions, characterized by the physical processes involved in the water vapor budget: the convective boundary layer, the outflow region of deep convective towers, and the region in between (the free troposphere). Deep convective towers take up the moist air within the convective boundary layer and generate hydrometeors. Some of the hydrometeors fall within the convective towers and some of them are carried to the upper troposphere, leading to the formation of widespread upper-level clouds. Upper-level clouds continue to generate precipitation, which falls into the subsaturated free troposphere and evaporates. (For clarity of discussion, we temporarily neglect the contribution from the dissipation of deep convective towers. As we will see later, this effect can be easily incorporated.) If a first-order description cannot be obtained using this idealized picture, we may conclude that there are some things fundamentally wrong with the idealization. If this picture can grasp the main features of the observed vertical structure, however, it may serve as a basis for a more complete representation. We will begin with the formulation of the equations for the water vapor budget and then discuss the parameterization of the moistening from the evaporation of hydrometeors.

a. *Equations for the water vapor budget*

Within the upper boundary layer (the outflow region of the deep convective towers) the supply of moisture is from the detrainment from these towers. The primary sink of moisture is the formation of upper-level clouds and the associated precipitation. The moisture budget of the outflow may be written as

$$M_{dc}q_{z_t} + R_{z_t} = S_{dc} \tag{3}$$

in which

$$S_{dc} = \int_{z_t}^{z_t^+} -\frac{dM_{dc}}{dz}(q^* + l^*)dz;$$

z_t^+ and z_t are the top height and base height of the outflow; M_{dc} is the convective mass flux within the deep convective tower, q^* is the saturation mixing ratio, and l^* is the ice/water content of the air detrained from the deep convective towers. Thus, S_{dc} is the total moisture input from the deep convective towers, ρR_{z_t} is the precipitation flux at the base of the outflow, q_{z_t} is the area mean water vapor mixing ratio, and $M_{dc}q_{z_t}$ is the water vapor flux at the base of the outflow. It is believed that l^* can be orders of magnitude larger than q^* in the upper troposphere. Therefore, Eq. (3) suggests that a significant precipitation flux is needed to keep the outflow subsaturated.

We further divide the outflow into two regions: the upper-level clouds and their clear air environment. The water vapor budget for the clear air environment can be written as

$$\rho E_{uc} + \rho E_{dc} + M_c\frac{dq}{dz} = 0; \tag{4}$$

M_c is the net large-scale subsidence in the clear air environment [since the model here is one dimensional (averaged over the Hadley domain), M_c is also the net convective mass flux], q is the water vapor mixing ratio in the clear environment, ρE_{uc} is the moistening from the upper-level clouds, and ρE_{dc} is the moistening from the deep convective towers.

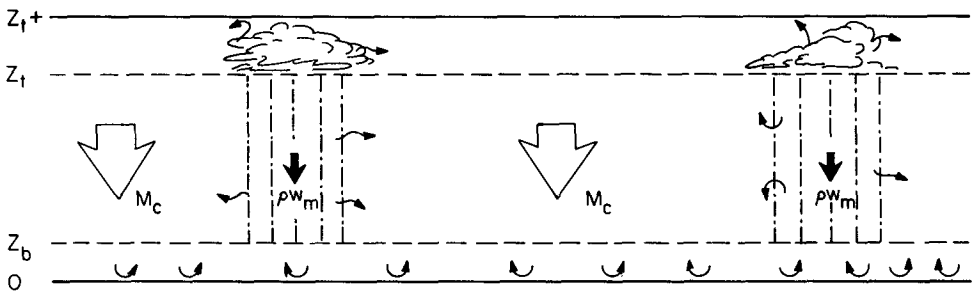

FIG. 10. A schematic illustration of the model structure. For clarity, the deep convective tower is not drawn. z_{t^*} is the tropopause height, z_t is the base height of the outflow, and z_b is the height of the convective boundary layer. M_c is the downward mass flux in clear sky, and ρw_m is the downward mass flux within the area covered by precipitation.

We assume that all the detrained water substance from the deep convective towers is directly used to feed the upper-level clouds. Then $E_{dc} = 0$ (note that the dissipation of deep convective towers is temporarily ignored). Equation (4) is simplified as

$$\rho E_{uc} + M_c \frac{dq}{dz} = 0. \tag{5}$$

In the free troposphere, the source of water vapor is from the evaporation of the precipitation. Since the precipitation from upper-level clouds is a cloud or mesoscale phenomenon, it is expected to generate entities that are distinct from the large-scale mean flow in terms of vertical velocity, density, and water content. Therefore, we have to distinguish the region covered by precipitation from the region free of precipitation (we will discuss some details of the relevant physical processes later on). Let M_c denote the net large-scale subsidence in the clear air and E_r the moisture input from the region covered by precipitation; then we have

$$M_c \frac{dq}{dz} + \rho E_r = 0 \tag{6}$$

for

$$z_t > z > z_b,$$

where z_t is the effective base height of the outflow of deep convective towers, z_b is the height of the surface convective boundary layer, q is the water vapor mixing ratio in the clear air environment, and E_r is the moistening supplied by the evaporation of precipitation.

When the fractional cover of the clouds is very small, the above equations can also be regarded as the area mean budget equation (see the Appendix). Since shallow convection within the convective boundary layer may be regarded as the natural extension of the turbulence driven by surface fluxes, further detailed separation between the dry boundary layer and the cloudy boundary layer will not add physical significance to our discussion. Furthermore, shallow clouds within the convective boundary layer (i.e., below the trade inversion) hardly precipitate. Therefore, to first order their effect in transporting water vapor may be parameterized as downgradient diffusion. In such a treatment we need not distinguish the shallow nonprecipitating clouds from their clear air environment. Let M_c denote the subsidence within the boundary layer; then the water vapor budget may be written as

$$M_c \frac{dq}{dz} + \frac{d}{dz}\left(K\rho \frac{dq}{dz}\right) = 0 \tag{7}$$

for

$$z \leqslant z_b,$$

where z_b is the height of the convective boundary layer and K is the diffusion coefficient.

If one's aim is to produce a realistic vertical structure of the water vapor mixing ratio, the surface value may be chosen as the observed value. Then the boundary conditions for the water vapor equations (5), (6), and (7) may be written

$$q|_{z=0} = q_0 \tag{8}$$

$$q|_{z=z_t^+} = q_t; \tag{9}$$

q_0 and q_t are the water vapor mixing ratio at the surface level and the tropopause level.

When the value of surface air mixing ratio is also a variable to be predicted, the surface boundary condition may be formulated as follows:

$$M_c(q_0 - q(z_b)) = c_d U\rho(q^*(T_s) - q_0), \tag{10}$$

which is a statement of the moisture budget of the convective boundary layer. The left side of this equation is the net loss of water vapor due to dynamic transport, and the right side is a parameterization of surface evaporation based on bulk aerodynamic formulas; c_d is the aerodynamic drag coefficient and U is the frictional velocity.

There are two other implicit boundary conditions, which are the continuity of water vapor content across 1) the interface between the outflow region and the free troposphere and 2) the interface between the free troposphere and the convective boundary layer.

The division into three regions may not be as clear in reality as in our model. The height of the convective boundary layer varies within the tropics and is not well defined in the ITCZ. Averaged over the whole tropics, the height of the convective boundary layer may be chosen as 2 km (Betts and Ridgway 1989). The mean thickness of the outflow of the deep convective tower is less well documented. The base height for cirrus clouds may give a useful indication. Based on London (1957), the base height for cirrus clouds is about 10 km. Therefore, the region in between the convective boundary layer and the outflow of deep convective towers occupies the bulk of the troposphere, which is our focus here.

b. Determination of the large-scale subsidence induced by deep convection

An estimate of M_c can be obtained by considering the energy budget of the large-scale subsidence. Away from the trade-wind boundary layer (where turbulent mixing may supply considerable sensible heat), the energy budget may be written as

$$M_c \frac{ds}{dz} - R_c = 0, \tag{11}$$

where s is the dry enthalpy and R_c is the net radiative cooling (infrared cooling plus solar heating). The lateral transfer of heat from deep convection to the sub-

siding air in the clear environment is assumed to be negligible (further discussions and a more rigorous derivation are presented in the Appendix).

Figure 11 shows the M_c profile in January deduced from Eq. (11). The temperature profile is from Oort (1983). Radiative cooling is taken from Dopplick (1972). In the boundary layer, M_c unexpectedly increases downward, presumably because sensible heating has been inappropriately neglected there. Rather than attempt to specify sensible heating in the boundary layer in detail, we will, for convenience, simply take M_c as constant with height within the convective boundary layer.

c. *A simple parameterization of the moistening from the upper-level clouds and their precipitation*

Upper-level clouds moisten their environment through evaporation of cloud water and mixing of the saturated cloud air into the environment. The bulk effect of this moistening is to bring the atmosphere to saturation, as is the bulk effect of the evaporation of hydrometeors falling from the base of upper-level clouds. Therefore, a simple, straightforward way to parameterize E_{uc} and E_r is through linear approximations,

$$E_{uc} = \alpha_c(q^* - q) \tag{12}$$

$$E_r = \alpha(q^* - q), \tag{13}$$

where q^* is the saturation value of water vapor mixing ratio (with respect to ice above the melting level) and q is the water vapor mixing ratio. Here α_c^{-1} is the time scale of moistening for upper-level clouds, α^{-1} is the time scale of moistening due to evaporation of precipitation, and α and α_c are related to the total moisture input into the upper-level clouds by deep convective towers (S_{dc}) and the precipitation flux at the base level of upper-level clouds ($R(z_t)$) by

$$\alpha_c = \frac{S_{dc} - R_{z_t}}{\int_{z_t}^{z_t^+} \rho(q^* - q)dz} \tag{14}$$

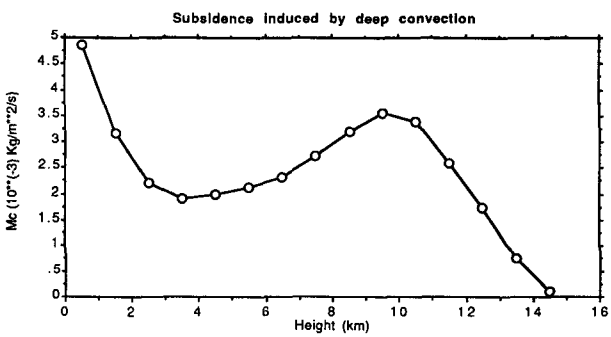

FIG. 11. Deep cloud induced subsidence deduced from the energy budget (in units of 10^{-3} kg m^{-2} s^{-1}).

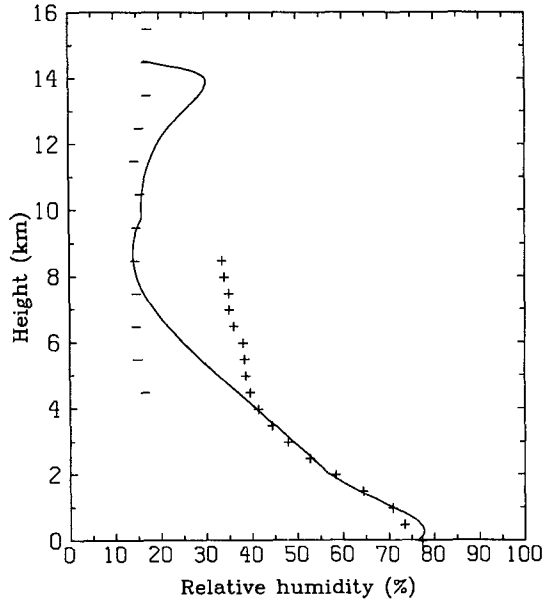

FIG. 12. The simulated vertical structure of the tropical tropospheric relative humidity in January. Relative humidity is with respect to liquid water. The solid curve is the model simulation; "+" and "−" represent the conventional and satellite data, respectively. The temperature profile used in this simulation is also from Oort (1983). Parameters are z_{t^+} = 14.5 km, z_t = 9.7 km, z_b = 2.0 km, K = 3.4 m^2 s^{-1}, α^{-1} = 14 days, and α_c^{-1} = 7 days. The corresponding S_{dc} = 1.24 kg m^{-2} day^{-1}, and R_{z_t} = 1.21 kg m^{-2} day^{-1}.

and

$$\alpha = \frac{R(z_t)}{\int_{z_b}^{z_t} \rho(q^* - q)dz}, \tag{15}$$

where ρ is the air density. It is assumed that precipitation flux at the level of z_b, R_{z_b}, can be ignored compared with R_{z_t}.

This simple parameterization straightforwardly relates the moistening by the upper-level clouds and the precipitation they generate to the amount of upper-level clouds (i.e., the total moisture input from deep convective towers to the upper boundary layer) and the amount of precipitation generated by upper-level clouds. The parameterization is closed either by coupling a deep cloud model that gives S_{dc} and a model for upper-level clouds that gives R_{z_t} or with specified S_{dc} and R_{z_t}. An advantage of this parameterization is that all parameters involved can be directly verified by observations. In the following section, we check this parameterization by estimating the observed vertical distribution of water vapor.

d. *Simulation of the observed vertical distribution of water vapor*

A simulation of the vertical distribution of water vapor is presented in Fig. 12. In our simulation, S_{dc}

and R_{z_t} are specified. This is equivalent to specifying α and α_c [Eqs. (14) and (15)]. This is sufficient for our present purpose in estimating the observed distribution. Between z_t and z_{t^+}, Eq. (5) is used for the water vapor budget; q_0 and q_t are fixed at the observed values. In general, a simulation with realistic features is obtained. This supports our interpretation for the observed tropical tropospheric water vapor distribution at least as concerns gross behavior. Some discrepancy with observational data is expected, given the simplicity of parameterization and the uncertainties in the observational data. Figure 13 shows the parametric dependence of tropical tropospheric relative humidity as depicted by this model. Note that above the boundary layer the effect of increasing α is equivalent to decreasing M_c. Figure 13 demonstrates that the relative humidity is related to the circulation and the microphysics of precipitation and can change if the processes change. (In these sensitivity studies, α_c is assumed to be proportional to α as it should because R_{z_t} is expected to be proportional to S_{dc}. Here α_c is assumed to be larger than α considering that the precipitation downdrafts may be subsaturated but upper-level clouds are constituted by saturated updrafts and downdrafts. The physical meaning of these two parameters will be discussed further in the following section.)

This model supplies a quantitative context for evaluating the roles of the relevant physical processes as highlighted by observation. However, the physical processes associated with moistening by the upper-level clouds and their precipitation are buried in the constant coefficients, α^{-1} and α_c^{-1}, the time scales for moistening. We will discuss these physical processes below.

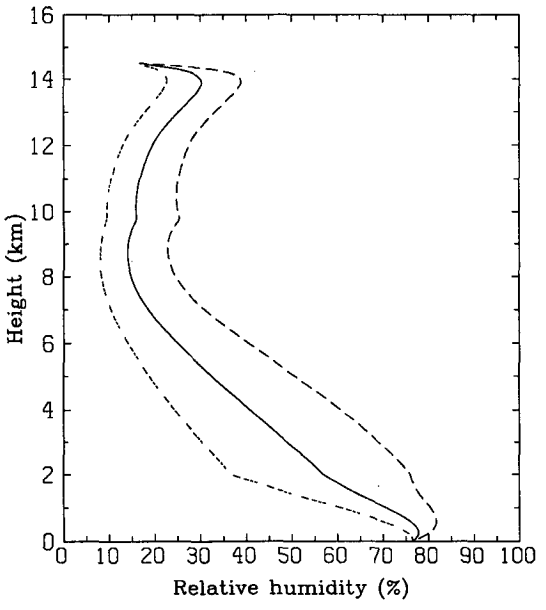

FIG. 13. The sensitivity of the simulated vertical structure of the tropical tropospheric relative humidity to changes in α and α_c. Relative humidity is with respect to liquid water. Solid line: $\alpha^{-1} = 14$ days and $\alpha_c^{-1} = 7$ days. The corresponding $S_{dc} = 1.24$ kg m^{-2} day^{-1} and $R_{z_t} = 1.21$ kg m^{-2} day^{-1}. Long-dashed line: $\alpha^{-1} = 7$ days, $\alpha_c^{-1} = 3.5$ days. The corresponding $S_{dc} = 1.68$ kg m^{-2} day^{-1} and $R_{z_t} = 1.62$ kg m^{-2} day^{-1}. Short-dashed line: $\alpha^{-1} = 28$ days and $\alpha_c^{-1} = 14$ days. The corresponding $S_{dc} = 0.796$ kg m^{-2} day^{-1}, $R_{z_t} = 0.775$ kg m^{-2} day^{-1}. Other parameters are $z_{t^+} = 14.5$ km, $z_t = 9.7$ km, $z_b = 2$ km, $K = 3.4$ m^{-2} s.

e. *The physical processes buried in α and α_c*

1) PRECIPITATION DOWNDRAFTS AND THEIR LIFE CYCLE

Precipitation processes in the tropics are largely cloud-scale and mesoscale phenomena. When the lateral dissipation is a much slower process than the evaporation of hydrometeors, the evaporation of precipitation may establish a considerably moister local environment and the cooling associated with evaporation and precipitation loading will generate negatively buoyant currents. This seems to be true in the tropical atmosphere. Let p, T, and RH represent respectively the pressure, temperature and relative humidity of the environment in which an ice crystal with a radius r evaporates, and let τ represent the time it takes for the ice crystal to completely evaporate. The following numbers may serve as a quick reference: for $p = 600$ mb, $T = 273.15$ K, RH = 90%, and $r = 0.1$ mm, $\tau = 14$ min; for $p = 200$ mb, $T = 233.00$ K, RH = 90% and $r = 0.1$ mm, $\tau = 137$ min. The lateral diffusion has the time scale of L^2/D, where L is the horizontal scale of the area covered by the precipitation and D is the diffusion coefficient. For $L = 10$ km, and D as large as 5.0 m^2 s^{-1} (which may be regarded as a characteristic value for boundary-layer turbulence), $L^2/D \sim 3.4 \times 10^5$ min. This will no doubt enhance the ability of precipitation to survive in a subsaturated mean environment. Here it is worth recalling Braham's observation (Braham and Duran 1967) that ice crystals falling from cirrus can survive 15 000 feet (from 250 mb to 600 mb) in a mean environment with a relative humidity less than 30% (given by the sounding data). To parameterize the moisturization from the precipitation falling in a subsaturated environment, one has to take into account the fact that the precipitation flux generates small-scale precipitation downdrafts.

It should also be noted that precipitation downdrafts appear to moisten the environment mainly when they dissipate. When the precipitation penetrates downward, the exchange between the downdrafts and the mean environment is limited in view of the unusual survival ability of the precipitation as observed by Braham and Duran (1967). This can also be shown by the following estimates. For a downdraft with a moderate vertical velocity, 0.05 m s^{-1}, the time for an air parcel in the downdraft to descend 10 km is 2.0×10^5 s. The lateral dissipation time scale is 2.0×10^7 s for a turbulent downdraft with a half-width 10^4 m.

In view of the above, the moistening of the large-

scale mean flow from the precipitation flux may be written as

$$E_r = \frac{\sigma}{\tau}(q_m - q), \tag{16}$$

where σ represents the fractional area of dissipating clouds, τ is the time scale of dissipation, q_m is the water vapor mixing ratio of the dissipating downdrafts, and q is the water vapor mixing ratio of the large-scale flow. A reasonable assumption for q_m is that it lies in between q^* and q. A linear approximation may be written as $q_m = (1 - c)q^* + cq$, with moistening written as $E_r = c\sigma/\tau(q^* - q)$. Thus, $\alpha = \sigma/\tau c$.

When the downdraft dissipates, the temperature of the downdraft air differs little from the environment it merges into. Thus, for $q_m > q$, the equivalent potential temperature of the downdraft air has to be larger than the environment. Since the minimum environmental equivalent potential temperature occurs in the middle troposphere, to be able to moisten the environment, the downdraft air has to originate from the upper troposphere. This again suggests the importance of the upper-level precipitation.

Upper-level clouds consist in saturated updrafts and downdrafts; therefore, the moistening from upper-level clouds may also be written in the above form with the replacement of q_m by q^*:

$$E_c = \frac{\sigma}{\tau}(q^* - q). \tag{17}$$

Thus, $\alpha_c = \sigma/\tau$.

The simple parameterization with a constant α is equivalent to assuming that the precipitation downdrafts have a constant relative humidity. A more realistic approach is to explicitly calculate the vertical distribution of q_m by coupling a model for the precipitation downdraft. Such a treatment immediately reveals the potential importance of details of the precipitation particles, such as the total water content and the size distribution of precipitation particles, in affecting the vertical distribution of water vapor in the large-scale flow.

2) THE ROLE OF THE SIZE SPECTRUM AND WATER CONTENT OF HYDROMETEORS

The budget of the hydrometeors and water vapor within the precipitation downdraft may be represented by the following equations,

$$\frac{d[(V_t + w_m)\rho]\rho_r}{dz} - \rho E_{mr} = 0, \tag{18}$$

$$\rho w_m \frac{dq_m}{dz} + \rho E_{mr} = 0, \tag{19}$$

for the free troposphere; ρ_r and q_m are the mixing ratios for hydrometeor and water vapor, respectively; ρ is the density of the downdraft air and $\rho\rho_r$ is the hydrometeor water content; ρw_m is the mass flux within the precipitation downdrafts, which will be assumed to be constant with height; V_t and E_{mr} are, respectively, the mass-weighted mean terminal velocity and the evaporation rate of hydrometeors. The boundary conditions for ρ_r and q_m may be written as:

$$\rho_r(z_t) = h_c; \quad q_m(z_t) = q^*(z_t), \tag{20}$$

where h_c is the mixing ratio of precipitating particles at z_t, the height of the upper cloud base where precipitation originates. At that level, the precipitation downdraft may be taken as saturated; $q^*(z_t)$ is the saturation mixing ratio of water vapor.

Assuming the size spectrum of the hydrometeors is exponential $N(r) = N_0 \exp(-\lambda r)$ (r is the radius of a hydrometeor and $N(r)dr$ is the number of hydrometeors with radii between r and $r + dr$ per unit volume), the evaporation rate of hydrometeors can be further written as

$$E_{mr} = -4\pi D C_v N_t \bar{r} \frac{1}{1 + \epsilon}(q_m - q^*), \tag{21}$$

where D is the molecular diffusion coefficient, q^* is the saturation water vapor mixing ratio,

$$\epsilon = \frac{D}{K}\frac{e_s(T)}{R_v T^2}\left(\frac{L}{R_v T} - 1\right)L,$$

R_v is the gas constant of water vapor, T is the temperature, $e_s(T)$ is the saturation pressure of water vapor, K is the coefficient of thermal conductivity of the air, L is the latent heat, $\bar{r} = B(\rho\rho_r)^{1/4}$ and $B = (8\pi N_0 \rho_i)^{-1/4}$, $\bar{r}$ is the mean radius of the hydrometeors, ρ_i is the density of the hydrometeors, $N_t = \int N(r)dr = N_0\bar{r}$. C_v is the ventilation coefficient that is related to the mean terminal velocity by $C_v = 0.78 + 0.28\,\mathrm{Re}^{1/2}$, $\mathrm{Re} = 2\bar{r}\rho V_t/\mu$ is the Reynolds number (Roger and Yang 1989), μ is the dynamic viscosity, V_t is the mass-weighted mean terminal velocity, $V_t = \int v_t(r)N(r)dr / \int m(r)N(r)dr$, and $v_t(r)$ and $m(r)$ are the terminal velocity and the mass of the hydrometeors with radius r. Taking $v_t(r) = kr$, the mass-weighted mean velocity can be related to the hydrometeor water content by $V_t = A(\rho\rho_r)^{1/4}$ where $A = 4k/(8\pi N_0\rho_i)^{1/4}$ (Mason 1971; Rogers and Yau 1989).

Ground level observations show that the size spectrum of continental rain can be well represented by an exponential form (Marshall and Palmer 1951). The upper-level precipitation spectrum is less well known. Observations of cirrus show that the size spectrum of ice crystals in the upper-level clouds can be represented by the sum of two exponential distributions (Heymsfield 1984). For our present purpose, such a form may be sufficient.

Numerical solutions for (18), (19), and (20) with different values for N_0 and h_c are presented in Figs. 14

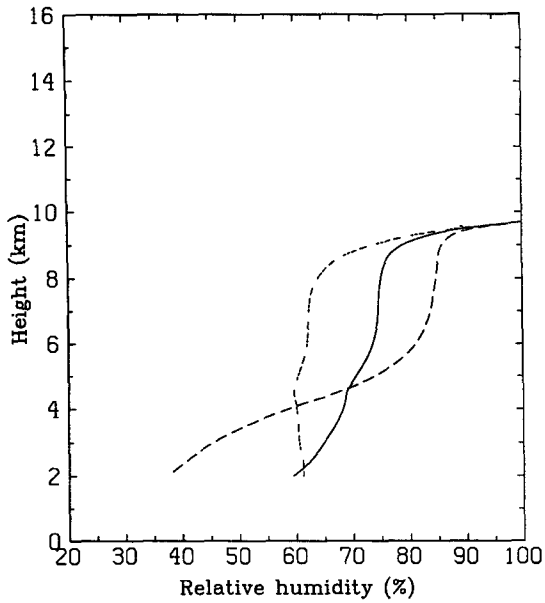

FIG. 14. Sensitivity of the relative humidity distribution within the precipitation downdraft to the change of spectrum of hydrometeors. Relative humidity here is with respect to liquid water. Parameters are z_t = 9.7 km, ρw_m = 0.2 kg m^{-2} s^{-1}, and h_c = 0.5 g kg^{-1}. Solid line: $N_0 = 0.8 \times 10^7$ m^{-4}. Long-dashed line: $N_0 = 0.8 \times 10^8$ m^{-4}. Short-dashed line: $N_0 = 0.8 \times 10^6$ m^{-4}.

and 15. (Note that the curves are for the relative humidity instead of the mixing ratio q_m.) The temperature within the downdraft cannot differ considerably from its environment when the downdraft is in its dissipating stage; therefore, it is assumed to be the same as that of the mean environment. It is apparent from the three curves in Figs. 14 and 15 that the vertical distribution of the relative humidity within the precipitation downdrafts is sensitive to the spectrum of the hydrometeors as well as to their mixing ratio (recall the mean radius $\bar{r} \sim N_0^{-1/4}$).

Since the profile of q_m is sensitive to the properties of the hydrometeors, so will the vertical distribution of water vapor of the large-scale flow [Eq. (16)] be. Its dependence on the size spectrum of the hydrometeors is shown in Fig. 16. In the calculation, Eqs. (13) and (12) are replaced by Eqs. (16) and (17), respectively, and q_m is given from the simple model for precipitation downdrafts. We see that precipitation downdrafts with smaller hydrometeors tend to moisten the upper troposphere more.

3) DISSIPATION OF DEEP CONVECTIVE TOWERS

Deep convective towers at the dissipating stage consist in downdrafts. Conceptually, we may parameterize their contribution to ambient humidity in the same way we parameterized the moistening from precipitation. If we view the upper-level clouds and the associated hydrometeors as an extension of deep convective towers, we may have a unified description of how deep convection moistens the large-scale flow in which it is embedded. Deep convection uses the moisture from the convective boundary layer to generate small-scale, spatially isolated moist regions. Water vapor in these isolated regions is then transported to the surrounding flow by diffusive and convective processes. The subsiding motion in the surrounding flow, induced by deep convection itself, constantly advects the water vapor downward to where it comes from: namely, the convective boundary layer.

4. Simulation of the horizontal variation of relative humidity in the Hadley domain

In this section, we introduce a two-dimensional model based on the one-dimensional model presented above in order to simulate the horizontal variation of water vapor in the Hadley domain. We will show that the decrease of relative humidity from the ITCZ to the subtropics throughout the free troposphere is due to the sharp decrease in the amount of hydrometeors deposited in the upper troposphere by deep convection and the relatively flat distribution of subsidence in between clouds.

The water vapor budget equation is given by Eq. (2). In the following discussion, we omit the zonal and time-mean symbols (i.e., overbar and brackets) for brevity. The horizontal transport term can be ignored compared with the term for the vertical transport. After

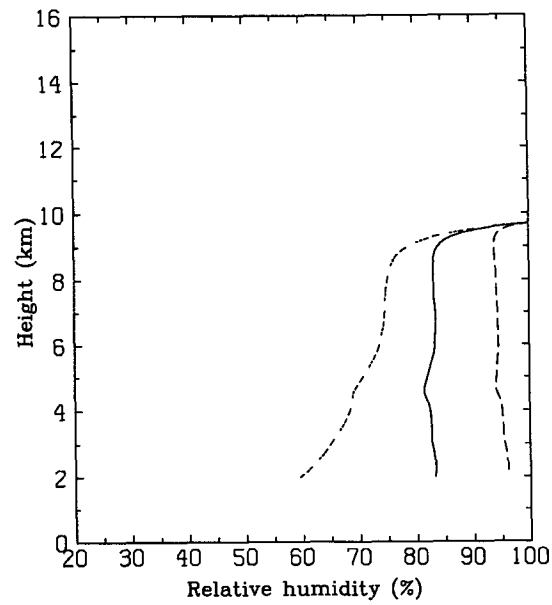

FIG. 15. Sensitivity of the relative humidity distribution within the precipitation downdraft to the water content of hydrometeors. Relative humidity is with respect to liquid water. Parameters are z_t = 9.7 km, ρw_m = 0.2 kg m^{-2} s^{-1}, and $N_0 = 0.8 \times 10^7$ m^{-4}. Solid line: h_c = 1.0 g kg^{-1}. Long-dashed line: h_c = 5.0 g kg^{-1}. Short-dashed line: h_c = 0.5 g kg^{-1}.

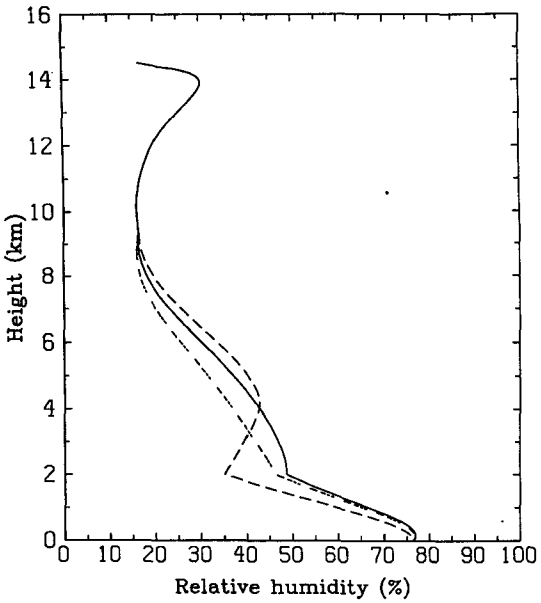

FIG. 16. Sensitivity of the mean relative humidity distribution to the relative humidity within the precipitation downdraft. Relative humidity is with respect to liquid water. The three curves shown correspond, each with the same notation, to the three precipitation downdraft relative humidity profiles of Fig. 14. Other parameters are $\tau/\sigma = 7$ days, $z_{t^+} = 14.5$ km, $z_t = 9.7$ km, $z_b = 2$ km, and $K = 3.4$ m^{-2} s^{-1}.

a new variable, $M_c^* = M_c - \rho w$, is introduced, Eq. (2) simplifies to

$$0 = M_c^* \frac{\partial q}{\partial z} + \rho E. \tag{22}$$

The latitudinal variation of M_c^* may be estimated from the energy equation:

$$M_c^* \frac{\partial S}{\partial z} - R_c = 0, \tag{23}$$

where S is the dry static energy and R_c is the net radiative cooling including both the solar heating and infrared cooling. The same approximations are made in deriving Eq. (23) as in deriving Eq. (22) (i.e., large-scale eddy transport and the horizontal advection by the mean circulation are ignored). This equation is valid only away from the boundary layer (where sensible heating by boundary-layer turbulence is considerable).

The meridional structure of M_c^* in January deduced from the above equation is plotted in Fig. 17; R_c is from Dopplick (1972) and S is from Oort (1983) (in Dopplick's calculation, clouds were also taken into account). Figure 17 shows that the latitude dependence of M_c^* is relatively weak. There is little evidence of the ITCZ. The subsidence appears relatively uniform throughout the cloud-free regions.

Again, we divide the atmosphere vertically into three regions: the outflow region, the free troposphere, and the convective boundary layer. In the free troposphere, $E = \alpha(y)(q^* - q)$, where y represents latitude. In the outflow region, $E = \alpha_c(y)(q^* - q)$; α_c is assumed to be proportional to α. In the convective boundary layer,

$$E = \frac{\partial}{dz}\left(K\rho \frac{\partial q}{dz}\right);$$

K is the bulk diffusion coefficient for the turbulent boundary layer. Now α and α_c are functions of latitude, and their meridional variation may be assumed proportional to the upper-level cloud cover [recall Eqs. (16) and (17)]. The meridional variation of upper cloud amount is well correlated with the variation of the middle- and upper-tropospheric relative humidity (see Fig. 18). The upper-level clouds are almost always associated with the outflow of storms (Liou 1986). The decrease of the upper cloud amount is, therefore, less likely a result of a decrease of the relative humidity of the environment and is more likely a cause—especially given the vertical separation between the 500-mb level and the upper-level clouds.

Figure 19 shows the simulated horizontal variation of relative humidity in the Hadley domain. The similarity with the observed distribution is apparent. This shows that the difference in the water vapor content between the convergence zone and the large-scale subsidence region may be due primarily to the distribution of hydrometeors.

The meridional distribution of hydrometeors from the ITCZ to the subtropics is largely controlled by the Hadley circulation. Deep convection tends to occur

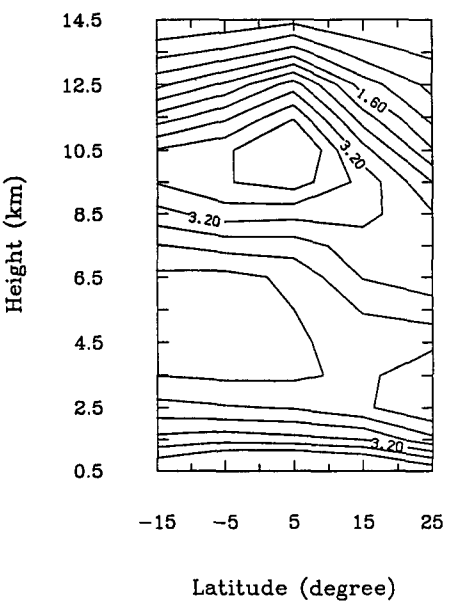

FIG. 17. The meridional distribution of M_c^* within the domain of the Hadley circulation (see text for further detail; unit is 10^{-3} kg m^{-2} s^{-1}).

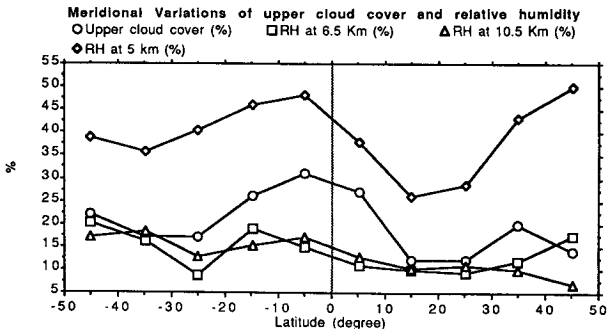

FIG. 18. The meridional variation of upper cloud cover and the variation of the tropical tropospheric relative humidity. Upper cloud cover is from Barton (1983). Relative humidity at 6.5 km and 10.5 km is calculated from SAGE II measurements (Rind et al. 1991). Relative humidity at 5 km is from Oort (1983).

where the sea surface temperature is highest. Accompanying the deep convection are large-scale circulations driven by the sea surface temperature gradient. The subsiding motion of the large-scale circulation suppresses convective motion elsewhere, that is, the subtropics. This is the reason for the decrease of the moisture source above the convective boundary layer as one moves from the ITCZ to the subtropics.

Clearly, the difference of water vapor content between the ITCZ and the subtropics is related to the existence and direction of the large-scale circulation. In a thermodynamic sense, the water vapor content of the air above the trade inversion over the subtropics is not directly related to the sea surface temperature immediately below; the air is subsiding and isolated from the boundary layer by a strong trade inversion. The inference by Rind et al. (1991), that upper-level humidity at any point is determined by the surface temperature at that point, ignores the interplay between the deep convection and the tropical zonal mean circulation and also ignores the vertical structure of the tropical convection.

5. Summary and discussion

By using a conceptual model for tropical convection and available data for water vapor, we investigated the maintenance of the tropical tropospheric water vapor distribution. Calculations were performed to see if the observed water vapor distribution could be explained in this simple context, and also to highlight some potentially important physical processes in determining the observed distribution and its sensitivity.

The observed profile of water vapor indicates that the large-scale subsiding flow has to be subject to moistening in the process of subsiding. The characteristic structures of the tropical circulation and budget studies suggest that the chief moisture source for the large-scale subsiding flow appears to be the evaporation of the hydrometeors transported to the upper troposphere by deep convective towers. Using a subsidence rate deduced from the energy budget and a simple parameterization of the moistening from the evaporation of hydrometeors, we are able to simulate the observed water vapor distribution. We also discussed the role of Hadley circulation in shaping the meridional variation of water vapor. We have contrasted our results with earlier suggestions. In particular, the suggestion of Lindzen (1990a,b) that the detrainment of saturated air from deep cumulus towers was a significant source has been shown to be inconsistent with the observed distribution of humidity. Related to this is our observation that both the observed pattern of large-scale subsidence outside of cumulonimbus towers and the absence of broad deep cloud cover throughout the tropics rule out the possibility of large-scale upward transport of water vapor from the boundary layer. Our study of the meridional distribution of water vapor within the Hadley domain showed that the decrease in humidity as one moved from the ITCZ was largely a result of the decrease in upper-level cloud cover rather than due to increasing subsidence outside of cumulus towers. The latter was found to be fairly uniform throughout the tropics.

For purposes of determining climate sensitivity, it is important to be able to calculate the upper-level water vapor. The present study shows that this is essentially tantamount to determining the amount of hydrome-

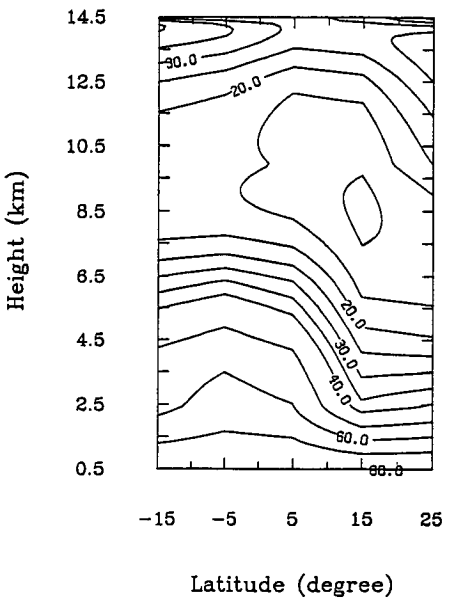

FIG. 19. A simulation of the horizontal variation of the tropical tropospheric relative humidity (with respect to liquid water) α and α_c are both assumed to be proportional to the upper-level cloud cover with $\alpha/\alpha_c = 2$. $z_t^* = 14.5$ km, $z_t = 9.7$ km, $z_b = 2.0$ km, and $K\rho_0/M_c = 2.0$ km in the convective boundary layer. The surface relative humidity is specified as 80%, and the specific humidity at 14.5 km is fixed as 4.3×10^{-3} g kg^{-1}. Within the convective boundary layer, M_c^* is assumed to remain constant with height.

teors in the upper troposphere. This quantity appears to be proportional to the strength of the updrafts of deep convective towers (Williams et al. 1992). This suggests an important role for the environmental CAPE (convective available potential energy) in determining the tropospheric water vapor content. It is the CAPE that determines the strength of the convective updraft. The environmental CAPE is a function of the entire vertical distribution of the tropospheric temperature. Thus, the present finding challenges the traditional notion that the tropospheric water vapor content is only dependent on the local temperature through the Clausius–Clapeyron equation. Note that there is no obvious reason to assume that a warmer climate necessarily has more CAPE. It is important, in this regard, to distinguish distinct climate regimes from local conditions. Above the trade cumulus boundary layer, tropical temperatures vary little horizontally. Therefore, local variations in CAPE are closely associated with variations in surface temperature. Different climate regimes, however, may also be associated with different distributions of temperature above the boundary layer. Such changes can affect CAPE for the entire tropics.

The life cycle of deep convective updrafts is also expected to be an important factor in determining the amount of hydrometeors present in the upper troposphere. If the updraft can persist longer, there will be more water substance transported to the upper troposphere. It is generally observed that the onset of precipitation signals the decay of the updraft. In a warmer climate, the surface air will likely contain more water vapor and the warm rain process will be more efficient. Consequently, the onset of rain may become faster (Fletcher 1962). An estimate based on the simplest continuous growth model, the Bowen model (see Bowen 1950; Fletcher 1962), was made (Fig. 20), which shows that the onset of rain can be 15% faster when surface temperature is increased by 2 K, and when the relative humidity of surface air is fixed as 80%.

The details of the moistening from the evaporation of hydrometeors are related to the dynamics of the development and decay of upper-level clouds and the associated precipitation processes for which we do not have adequate understanding. Observations and simple scaling analysis show that the evaporative cooling and the drag of precipitation generate currents that can penetrate deep into the large-scale flow and form small-scale, isolated regions of higher moisture content. The water vapor distribution in the large-scale flow is ultimately dependent on how water vapor flows from these small isolated regions to the surrounding flow and how these small regions dissipate and finally merge into the surrounding flow. Details such as the spectrum and water content of the hydrometeors in the small-scale precipitation downdrafts also appear to be important. These issues have not, so far, been given much attention. Proper models need to be developed for these

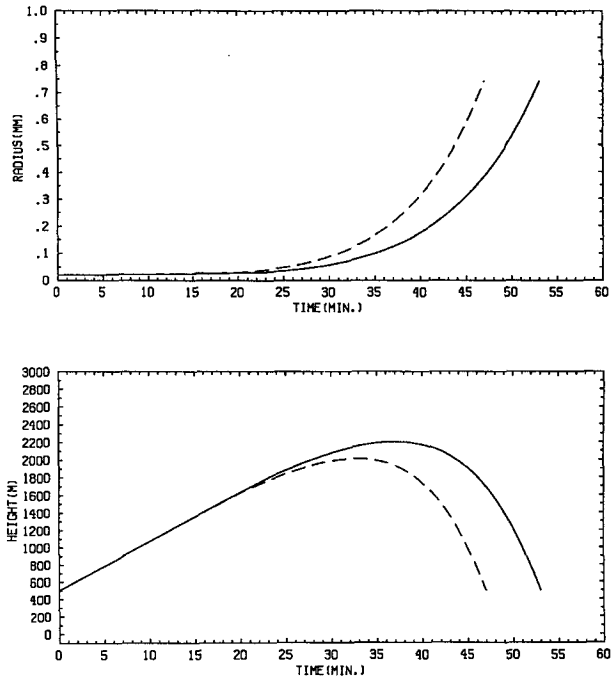

FIG. 20. Sensitivity of the growth of a raindrop in a constant updraft to the change of surface air temperature. Upper panel: growth of the raindrop as a function of time. Lower panel: trajectory of the raindrop. Solid line: surface air temperature is 300 K. Dashed line: surface temperature is 302 K. Surface relative humidity is 80% and is assumed constant. Cloud water content is assumed to be constant with height. For the surface temperature of 300 K, the cloud water content is chosen as 1 g m^{-3}. When surface temperature changes, the relative change of cloud water content is assumed to be the same as the relative change of the surface specific humidity. The size spectrum of cloud water is assumed to be uniform and not subject to change when surface temperature changes. The radius is chosen as 0.01 mm.

small-scale currents to simulate their interaction with the environment during their full life cycle. Unfortunately, we still lack appropriate models for the upward jet driven by the release of the latent heat and the downward current driven by the loading of precipitation and its evaporative cooling.

While it appears that precipitating upper-level clouds play a vital role in determining the tropospheric relative humidity throughout the free troposphere, they are also optically thick and their effect on albedo may offset their greenhouse effect (Ramanathan and Collins 1991). Further climate studies will have to address water vapor and clouds in a more internally consistent way. Here, we have provided a simple approach to connecting them.

The issue of the water vapor budget of the tropical troposphere and its sensitivity to global warming involves many physical processes with different temporal and spatial scales. It has to be attacked through a hierarchy of models, but more complex models should be based on simpler models to assure understanding. The main motivation of this work has been to provide

a simple framework for interpreting what has been observed about the large-scale distribution of water vapor, permitting us to highlight the important physical processes involved. The effort here is hopefully sufficient for this purpose, despite the crudity with which the individual physical processes have been treated.

Acknowledgments. This research was supported by the National Science Foundation under Grant ATM-8520354, and by the National Aeronautics and Space Administration under Grant NAGW-525. Helpful discussions with K. A. Emanuel, A. Plumb, P. Stone, E. R. Williams, and R. Prinn are gratefully acknowledged. We are also grateful to Dr. M. P. McCormick and Dr. E. W. Chiou of NASA for providing us the SAGE II data.

APPENDIX

Derivation of the Water Vapor and Heat Budget of a Large-Scale Flow Containing Moist Convection

The formulation of the water vapor and heat budget equations for large-scale flows containing moist convection has been approached by Kuo (1965, 1974) and Arakawa and Schubert (1974). The fundamental difference between the two approaches lies in their assumptions about the large-scale flow. Kuo essentially treated the large-scale flow as a turbulent flow where moist convection is not a distinguishable element. Naturally, the instantaneous mixing of clouds into the large-scale flow was assumed. In Arakawa and Schubert's approach the large-scale flow is divided into two regions, the moist convection and its environment. The flow in the environment is treated essentially as a laminar flow. In view of the fact that moist convective motion (turbulence) is usually confined to small regions and that moist convection transports mass primarily vertically, Arakawa and Schubert's formulation is more appropriate to atmospheric flows with scales much larger than the scale of moist convection (i.e., synoptic disturbances, the Hadley circulation, etc.). In Arakawa and Schubert's formulation, however, a steady plume model for moist convection is assumed, and the way the moist convection interacts with its environment is probably too limited to accurately describe the real atmospheric situation.

A straightforward generalization of Arakawa and Schubert's formulation is to replace the steady plume model by moist drafts (up and down) with a finite life cycle. By moist drafts, we here refer to small-scale entities associated with moist convection. They are spatially isolated and are distinguished from their environment by differences in density, vertical velocity, water content, and temperature. That is to say, they are out of equilibrium with their environment. These various differences usually coexist, but not always. Here, we focus on the difference in density (i.e., the buoyancy force).

We consider a large-scale flow with horizontal velocity $\mathbf{V}_h$ and density ρ. Small-scale moist drafts associated with moist convection are embedded in the flow (Fig. 21 presents a schematic illustration; the shaded area represents the moist drafts and the unshaded area is their environment.). Let E_{ci} represent the mass lost from the ith draft to its large-scale environment and E_e represent the mass lost from the environment to the moist drafts over a unit volume and time; we then have the following water vapor budget for the environment:

$$\frac{\partial}{\partial t}[(1-\sigma)\rho q_e] = -\frac{\partial}{\partial z}[(1-\sigma)\rho w_e q_e] - \nabla_2(\mathbf{V}_h \rho q_e) - E_e q_e + \sum_i E_{ci} q_{mi} + E_d, \quad (24)$$

where q_e is the water vapor mixing ratio of the environment, q_{mi} is the mixing ratio of water vapor of the air flowing out of the ith moist draft, $\mathbf{V}_h$ is the horizontal flow, and w_e is the vertical velocity in the environment. The sum $\sum_i$ is over all the moist drafts contained in a unit area; σ is the fractional area covered by the moist drafts; and E_d is evaporation of the ice or liquid water detrained into the environment from the moist drafts. Neither condensation nor sublimation is assumed to occur in the environment. The physical meaning of other terms in the above equation should be self-evident. The mass budget equations within the moist drafts and the environment are, respectively,

$$\frac{\partial}{\partial t}[(1-\sigma)\rho] = -\frac{\partial}{\partial z}[(1-\sigma)\rho w_e] - \nabla_2 \cdot (\mathbf{V}_h \rho) - E_e + \sum_i E_{ci} \quad (25)$$

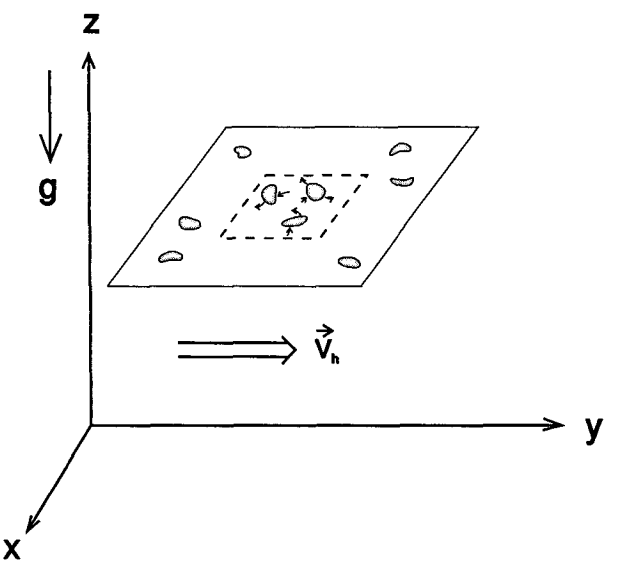

FIG. 21. A schematic illustration of a large-scale flow containing moist drafts associated with moist convection.

$$\frac{\partial}{\partial t}(\sigma\rho) = -\frac{\partial}{\partial z}(\rho \sum_i \sigma_i w_{ci}) + E_e - \sum_i E_{ci}. \quad (26)$$

The density difference between the air within the moist drafts and the environmental air is neglected in the above equations. Here σ_i is the fractional area covered by the ith draft and $\sigma = \sum \sigma_i$. With (26) and the Boussinesq approximation, $\partial\rho/\partial t = 0$, (24) can be rewritten as

$$(1-\sigma)\rho\frac{\partial q_e}{\partial t} = -\frac{\partial}{\partial z}[(1-\sigma)\rho w_e q_e] - \nabla_2(\mathbf{V}_h\rho q_e)$$

$$- q_e\frac{\partial}{\partial z}(\sum \sigma_i\rho w_{ci}) + \sum_i E_{ci}(q_{mi} - q_e) + E_d. \quad (27)$$

Defining a mean vertical velocity by $w = (1-\sigma)w_e + \sum_i \sigma_i w_{ci}$, and replacing $(1-\sigma)w_e$ in Eq. (27), we have

$$(1-\sigma)\rho\frac{\partial q_e}{\partial t} = -\frac{\partial}{\partial z}(\rho w q_e) - \nabla_2\cdot(\mathbf{V}_h\rho q_e)$$

$$+ \sum_i \rho\sigma_i w_{ci}\frac{\partial q_e}{\partial z} + \sum_i E_{ci}(q_{mi} - q_e) + E_d. \quad (28)$$

Using the mass conservation equation in the Boussinesq form, we get

$$\frac{\partial(\rho w)}{\partial z} + \nabla_2\cdot(\mathbf{V}_h\rho) = 0. \quad (29)$$

Then, we further have

$$(1-\sigma)\rho\frac{\partial q_e}{\partial t} + \rho w\frac{\partial q_e}{\partial z} + \rho\mathbf{V}_h\cdot\nabla_2(q_e)$$

$$= \sum_i \sigma_i\rho w_{ci}\frac{\partial q_e}{\partial z} + \sum_i E_{ci}(q_{mi} - q_e) + E_d. \quad (30)$$

In the case $\sigma \ll 1$, $q = (1-\sigma)q_e + \sigma q_c \sim q_e$. After introducing a variable $M_c = \sum_i \rho\sigma_i w_{ci}$, we obtain

$$\rho\frac{\partial q}{\partial t} + \rho w\frac{\partial q}{\partial z} + \rho\mathbf{V}_h\cdot\nabla_2(q)$$

$$= M_c\frac{\partial q}{\partial z} + \sum_i E_{ci}(q_{mi} - q) + E_d. \quad (31)$$

Replacing the sum of the last two terms by E and performing time and zonal averaging, we obtain Eq. (1) used in section 2.

Further parameterization of the last two terms in Eq. (30) is discussed in section 3 of the main text. Here we mainly point out the obvious problems in Arakawa and Schubert's widely used parameterization.

In Arakawa and Schubert's scheme, the moistening term was written as $\sum_i E_{ci}(q_{mi} - q) + E_d = \sum_i E_{ci}(q_{ci} + l_i^* - q)$; q_{ci} is the mixing ratio of water vapor and l_i^* is the water substance in liquid and solid form carried into the environment with the detrained air from the updraft. The problems with this treatment are the following. First, the evaporation of the detrained water will likely generate downdrafts. The downdrafts may penetrate a considerable distance until they reach a new neutral buoyancy level. Therefore, the detrained water substance from the updraft is not used to moisten the environmental air at the top of the updraft but at lower levels. Second, the detrained ice from deep convective towers may primarily take the form of upper-level clouds, which also do not immediately mix into the large-scale environment. This situation is typical of tropical deep convection (Houze 1989). Third, the idea that moist drafts (up or down) moisten their environment through detrainment at their limits is valid only when a steady plume model is applicable. The convective updrafts or downdrafts involved in moist convection have a very transient nature. In light of the starting plume model, the moist draft moistens the environment only when it begins to dissipate (Turner 1979, 1962), which suggests that the air within the drafts detrains at every altitude of the moist draft.

By the same procedure used to derive the water vapor budget, we can obtain the heat budget

$$\rho\frac{\partial s}{\partial t} + \rho w\frac{\partial s}{\partial z} + \rho\mathbf{V}_h\cdot\nabla_2(s)$$

$$= M_c\frac{\partial s}{\partial z} + \sum_i E_{ci}(s_{mi} - s) - LE_d, \quad (32)$$

where s is the dry enthalpy of the large-scale flow, s_{mi} is the dry enthalpy of the air lost from a moist draft to the environmental flow, E_d is the evaporation of liquid water and ice deposited from the moist drafts into the environment, and L is the latent heat. The sum is over all the moist drafts. The air from the moist draft will have the ambient density when it merges into its environment. This implies $s_{mi} \sim s$, and the heating or cooling associated with their difference can be neglected since the density difference is primarily caused by the temperature difference. The term LE_d is the part of evaporative cooling that does not lead to downdrafts, and it is expected to be small in the tropical troposphere. There are two reasons for this. First, when there is deep convection, the environmental temperature is close to neutral for moist-adiabatic ascent or descent. Second, the evaporation of detrained ice and liquid water is a much faster process than the lateral dissipation (see more detailed discussion in section 4). Thus, it is reasonable to assume that the convective heating due to moist convection is primarily realized by redistributing mass, that is, by inducing subsidence in its environment. With this assumption and for a flow subject to radiative cooling, (32) should be

$$\rho\frac{\partial s}{\partial t} + \rho w\frac{\partial s}{\partial z} + \rho\mathbf{V}_h\cdot\nabla_2(s) = M_c\frac{\partial s}{\partial z} - R_c, \quad (33)$$

where R_c represents the net radiative cooling.

REFERENCES

Arakawa, A., and W. H. Schubert, 1974: Interaction of a cumulus cloud ensemble with the large scale environment. Part I. *J. Atmos. Sci.*, **31**, 674–701.

Augstein, E., H. Schmidt, and F. Ostapoff, 1974: The vertical structure of the atmospheric planetary boundary layer in undisturbed trade winds over the Atlantic ocean. *Bound.-Layer. Meteor.*, **6**, 129–150.

Barton, I. J., 1983: Upper level cloud climatology from an orbiting satellite. *J. Atmos. Sci.*, **40**, 435–447.

Betts, A. K., 1990: Greenhouse warming and the tropical water vapor budget. *Bull. Amer. Meteor. Soc.*, **71**, 1465–1467.

——, and M. Ridgway, 1989: Climatic equilibrium of the atmospheric convective boundary layer over a tropical ocean. *J. Atmos. Sci.*, **40**, 435–447.

Bowen, E. G., 1950: The formation of rain by coalescence. *Austr. J. Sci. Res.*, **A3**, 192–213.

Braham, R. R., 1952: The water and energy budgets of the thunder storm and their relation to thunder storm development. *J. Meteor.*, **9**, 227–242.

——, and P. S. Duran, 1967: Survival of cirrus crystals in clear air. *J. Appl. Meteor.*, **6**, 1053–1061.

Broecker, W. S., and G. H. Denton, 1989: The role of ocean–atmosphere reorganization in glacial cycles. *Geochim. Cosmochim. Acta*, **53**, 2465–2501.

Chiou, E. W., M. P. McCormick, W. P. Chu, and G. K. Yue, 1990: Global distributions of cirrus determined from SAGE II occultation measurements between November 1984 and October 1988. Preprints, *Conf. on Cloud Physics*, San Francisco, Amer. Meteor. Soc., 513–517.

Danielsen, E. F., 1982: A dehydration mechanism for the stratosphere. *Geophys. Res. Lett.*, **9**, 605–608.

Dopplick, T. G., 1972: Radiative heating of the global atmosphere. *J. Atmos. Sci.*, **29**, 1278–1294.

Emanuel, K. A., 1991: A scheme for representing cumulus convection in large-scale models. *J. Atmos. Sci.*, **48**, 2313–2335.

Fletcher, N. H., 1962: *The Physics of Rain Clouds.* Cambridge University Press, 386 pp.

Gamache, J. F., and R. A. Houze, 1983: Water budget of a mesoscale convective system in the tropics. *J. Atmos. Sci.*, **40**, 1835–1850.

Gray, W. M., 1974: Cumulus convection and large scale circulations, I: Broad scale and mesoscale considerations. *Mon. Wea. Rev.*, **105**, 1171–1188.

Heymsfield, A., and C. M. R. Platt, 1984: A parameterization of the particle size spectrum of ice clouds in terms of the ambient temperature and the ice water content. *J. Atmos. Sci.*, **41**, 846–855.

Houze, R. A. Jr., 1989: Observed structure of meso-scale convective systems and implications for large scale heating. *Quart. J. Roy. Meteor. Soc.*, **115**, 425–461.

——, and A. K. Betts, 1981: Convection in GATE. *Rev. Geophys. Space Phys.*, **19**, 541–576.

Johnson, R. H., and G. S. Young, 1983: Heat and moisture budgets of tropical mesoscale anvil clouds. *J. Atmos. Sci.*, **40**, 2138–2147.

Lindzen, R. S., 1990a: Some coolness concerning global warming. *Bull. Amer. Meteor. Soc.*, **71**, 288–299.

——, 1990b: Response. *Bull. Amer. Meteor. Soc.*, **71**, 1465–1467.

——, and S. Nigam, 1987: On the role of sea surface temperature gradients in forcing low level winds and convergence in the tropics. *J. Atmos. Sci.*, **44**, 2440–2448.

——, and A. Y. Hou, 1988: Hadley circulations for zonally averaged heating centered off the equator. *J. Atmos. Sci.*, **45**, 2416–2427.

Liou, K. N., 1986: Influence of cirrus clouds on weather and climate processes: a global perspective. *Mon. Wea. Rev.*, **114**, 1167–1199.

Marshall, J. S., and W. M. Palmer, 1948: The distribution of rain drops with size. *J. Meteor.*, **5**, 165–166.

Mason, B. J., 1971: *The Physics of Clouds.* Clarendon Press, 671 pp.

Newell, R. E., J. W. Kidson, D. G. Vincent, and G. J. Boer, 1972: *The General Circulation of the Tropical Atmosphere and Interactions with Extratropical Latitudes*, Vol. 1. The MIT Press, 258 pp.

Ogura, Y., and H. R. Cho, 1973: Diagnostic determination of cumulus cloud population from observed large-scale variables. *J. Atmos. Sci.*, **30**, 1276–1286.

Oort, A. H., 1983: Global atmospheric circulation statistics, 1958–1973. NOAA Prof. Paper 14, Rockville, MD., NOAA, U.S. Department of Commerce. 180 pp.

Ramanathan, V., and W. Collins, 1991: Thermodynamic regulation of ocean warming by cirrus clouds deduced from observations of the 1987 El Niño. *Nature*, **351**, 27–32.

Riehl, H., 1979: *Climate and Weather in the Tropics.* Academic Press, 611 pp.

——, and J. S. Malkus, 1958: On the heat balance in the equatorial trough zone. *Geophysica* **6**, 503–538.

——, and ——, 1979: The heat balance of the equatorial trough zone, revisited. *Contrib. Atmos. Phys.*, **52**, 287–305.

——, T. C. Yeh, J. S. Malkus, and N. E. Laseur, 1951: The north east trade wind of the Pacific Ocean. *Quart. J. Roy. Meteor. Soc.*, **77**, 598–526.

Rind, D., E. W. Chiou, W. Chu, J. Larsen, S. Oltmans, J. Lerner, M. P. McCormick, and L. McMaster, 1991: Positive water vapor feedback in climate models confirmed by satellite data. *Nature*, **349**, 500–503.

Rogers, R. R., and M. K. Yau, 1989: *A Short Course in Cloud Physics.* Pergamon Press, 293 pp.

Sarachik, E. S., 1978: Tropical sea surface temperature: an interactive one-dimensional atmosphere-ocean model. *Dyn. Atmos. Oceans*, **2**, 455–469.

Schneider, E. K., 1977: Axially symmetric steady-state models of the basic state for instability and climate studies. Part II: Nonlinear calculations. *J. Atmos. Sci.*, **34**, 280–296.

Starr, D. O'C., and S. H. Melfi, 1991: The role of water vapor in climate. NASA Conf. Publication 3120. NASA Goddard Space Flight Center, 49.

Sun, D. Z., and R. S. Lindzen, 1992: Negative feedback of water vapor inferred from the mountain snowline record. *Ann. Geophys.*, submitted.

Turner, J. R., 1962: The starting plume in neutral surroundings. *J. Fluid Mech.*, **13**, 356–368.

——, 1979: *Buoyancy Effects in Fluids.* Cambridge University Press, 368 pp.

Williams, E. R., S. A. Rutledge, S. G. Geotis, N. Renno, E. Rasmussen, and T. Rickenbach, 1992: A radar and electrical study of tropical "hot towers." *J. Atmos. Sci.*, **49**, 1386–1395.